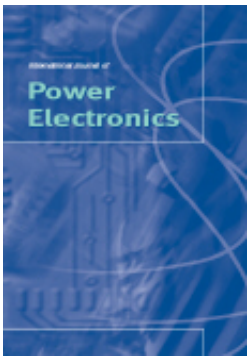


**International Journal of Power Electronics**

ISSN online: 1756-6398 - ISSN print: 1756-638X
https://www.inderscience.com/ijpelec

# Single switch high voltage gain DC-DC converter for renewable energy applications

Karri V.V. Satyanarayana, Rakesh Maurya

**DOI:** 10.1504/IJPELEC.2024.10055583

**Article History:**

| | |
|---|---|
| Received: | 18 May 2022 |
| Last revised: | 23 December 2022 |
| Accepted: | 09 January 2023 |
| Published online: | 23 December 2023 |

# Single switch high voltage gain DC-DC converter for renewable energy applications

Karri V.V. Satyanarayana

Department of Electrical Engineering,
Institute of Technology,
Nirma University,
Ahmedabad, Gujarat 382481, India
Email: karri.satyanarayan@nirmauni.ac.in

Rakesh Maurya*

Department of Electrical Engineering,
Sardar Vallabhbhai National Institute of Technology,
Surat 395007, India
Email: rmaurya@eed.svnit.ac.in
*Corresponding author

**Abstract:** In a DC microgrid, the integration of renewable energy sources (RES) is necessary to meet the regular load demands of electricity. The generating voltage of RES are at low level. So, the requirement of high voltage gain converters is essential for the function of grid-forming or grid-feeding converters. This paper presents a non-isolated DC-DC converter with features of high voltage gain and high efficiency. This converter functioning with single switch and passive components in which two inductors and one capacitor are connected in parallel/series during ON state/OFF state of switch respectively. The detailed operation of this converter under CCM and DCM modes with necessary voltage and current waveforms are discussed. The efficiency analysis and state space average modelling of proposed converter is presented. The comparative analysis of single switch topologies is also presented with few selected converters. The theoretical analysis of proposed converter is validated through prototype model designed in laboratory environment and obtained results are presented.

**Keywords:** switching losses; high voltage gain; duty ratio; continuous conduction mode and efficiency.

**Reference** to this paper should be made as follows: Satyanarayana, K.V.V. and Maurya, R. (2024) 'Single switch high voltage gain DC-DC converter for renewable energy applications', *Int. J. Power Electronics*, Vol. 19, No. 1, pp.1–23.

**Biographical notes:** Karri V.V. Satyanarayana received his BTech and MTech in Electrical Engineering in 2006 and 2012 from Kakinada Institute of Engineering and Technology, JNTU Hyderabad, A.P and BVC Engineering College, JNTU Kakinada, A.P. He is currently serving as an Assistant Professor in the Department of Electrical Engineering, Nirma University, Ahmedabad, India. His research interests are DC microgrid, DC-DC converters and multilevel inverter.

Rakesh Maurya received his BTech in Electrical Engineering from the Kamla Nehru Institute of Technology, Sultanpur, India, in 1998, MT in Power Electronics and Electric Drive and PhD in Electrical Engineering from the Indian Institute of Technology Roorkee, Roorkee, India in 2002 and 2014 respectively. He is currently serving as an Associate Professor in the Department of Electrical Engineering, Sardar Vallabhbhai National Institute of Technology, Surat, India. His current research interests include design of switching power converters, high power factor AC/DC converters, hybrid output converters, improved power quality converters for battery charging applications, power quality problems, advanced electric drives and applications of real-time simulator for the control of power converters. He is a member of IEEE and life member of System Society of India.

## 1 Introduction

Nowadays renewable energy resources like fuel cells, wind energy and solar are freely available in nature and they are intermittent in nature. The generating voltage levels of RE sources such as fuel cells and photovoltaic modules are at low level. In order to meet the regular demand of supply for customers, there is a need of integration of these RESs in form of DC micro-grids. In view of the generated voltages of RESs and requirement of DC micro grid, there is necessity of high gain converter with features of low loss and high efficiency to meet the DC load demands (Eghtedarpour and Farjah, 2014; Carrasco et al., 2006). High gain converters, not only used for integration of RE sources, they are also used for many applications like some medical equipments, battery backup for uninterruptible power supplies, high intensity discharge lamp ballasts for automobile headlamps and electric traction (Bryant and Kazimierczuk, 2007; Wu et al., 2008). When extracting the maximum power from the PV panel, the converter should maintain continuous input current with less ripples. On the other hand, if the PV current has too much ripple in such low-voltage systems, the maximum power point tracker (MPPT) algorithm cannot extract maximum power from the panel. Further, for proper functioning of fuel cells, the regulation of output voltage is mandatory. Thus, converter needs to maintain continuous input current with less ripples. The dynamic response of the system also depends on continuous input current. So, for DC microgrid applications, in order to increase system overall efficiency and reliability, the converter should transfer high voltage gain with continuous low ripple input current and maximise the power capture (Park et al., 2010; Ardi et al., 2018). Thus, the utilisation of buck-boost converters is limited. These converters are divided to isolated (Mantovanelli and Barbi, 1996) and non-isolated (Li and He, 2011). If two sides of the circuit cannot be connected to a common ground, must be used isolated type, but if isolation is not required, the non-isolated type is used which structure is simpler and more comfortable design, also non-isolated type has higher efficiency and lower volume.

The traditional boost converter offers high voltage gain at extreme duty cycles but recovery of diode is very difficult and yields high voltage stress on switch. This causes converter conduction losses are increased and decreases the efficiency (Wai et al., 2007; Hart, 2011). In recent days, more research works are carried out on high gain converters. Many isolated high gain and high efficiency converters are presented in literature (Ajami et al., 2015; Chen et al., 2015; Mohammadi et al., 2014; Nguyen et al., 2018). These

converters voltage gain can be increased by increasing the turns ratio of high frequency transformer. This leads to increase the weight and volume of converter. Moreover, the main disadvantage of this converter includes high voltage spikes during turning off of the switching devices due to leakage inductance of transformer. The mitigation of switching spikes is to be carried out by clamping circuit and recycling the energy. Hence, additional clamping circuit increases the cost, complexity and reduces the converter efficiency (Salvador et al., 2018). By reducing resonance between leakage inductance and parasitic capacitance of semiconductors, these isolated converters can reduce the maximum voltage blocking requirement. The converter proposed in Lakshmi and Hemamalini (2018) offers high voltage gain with two different duty cycles. This converter comprises of three switching elements and two inductors. These three switching elements are operating in two different duty cycles. So, this converter control is very difficult when it is used for photovoltaic systems because most of the MPPT control techniques are generating single duty cycle.

In recent times, non-isolated high gain converters are more popular because of their simple structure, compact size, low cost and improved efficiency compared to isolated high gain converters (Tofoli et al., 2015). These high gain non-isolated converters are categorised into two groups namely coupled inductor DC-DC converters and non-coupled inductor DC-DC converters (Salvador et al., 2018; Berkovich and Axelrod, 2011). Former converters offer high gain by increasing number of turns of inductors and similarly to isolated converters which yield high voltage spikes during turning off the switching devices. This issue can be overcome by adding an additional clamping circuit to recycle the energy and improves the efficiency. Hence circuit complexity and cost of the circuit is increased (Li and He, 2011). On the other hand, non-coupled converters achieve high voltage gain through additional technique like voltage multipliers (Luo and Ye, 2004; Prudente et al., 2008) cascaded converters (Baddipadiga and Ferdowsi, 2017) switched capacitors and switched inductors (Axelrod et al., 2008; Forouzesh et al., 2017) and combination of these techniques (Tofoli et al., 2012). Switched capacitor converters consist of only capacitors, switches and diodes. Switched-capacitor (SC) circuits can provide high step-up ratios depending on the number of capacitors used in the SC cell. These converters, do not involve inductive elements and isolated transformers. This leads to minimise the noise and radiated EMI. However, these converters utilise the more components and several voltage multipliers. This causes increased the circuit complexity, cost and reduce the efficiency of converter. Furthermore, several SEPIC converter based high gain converters are presented in Lee and Do (2018). Moradpour et al. (2018), Ardi and Ajami (2018). The converter Lee and Do (2018), offers lossless snubber circuit and ripple free input current with high gain compared to conventional boost converter. The advantages of ripple free input current are already discussed. The converters Moradpour et al. (2018), Ardi and Ajami (2018) are designed with isolated transformers and coupled inductors. However, these converters suffered from the above-mentioned drawback of isolated converters and coupled inductors. The SEPIC based converters Zhu and Luo (2008), Banaei and Sani (2018) are designed without isolation transformers and coupled inductors. These follows the afore mentioned advantages of non-coupled inductors and non-isolated transformers. However, these converters gain is still low. Some of the PWM converters are presented by the active clamp (Choi et al., 2010), which by using one or more additional switches and passive elements, zero voltage switching (ZVS) condition is provided for all switches. But these converters have duty cycle losses and the current stresses are high.

The main objective of this paper is to develop the high voltage gain converter which is suitable for integration of renewable energy resources to the DC micro-grid. Additionally, it has features of less component count, high efficiency, low voltage stress on devices and low losses as compared with its equivalent other reported converters Gules et al. (2014), Banaei et al. (2014), Ismail et al. (2008). High gain soft switching converter for photovoltaic system is presented in Vesali et al. (2021). This topology involved the coupled inductors. The disadvantages of coupled inductors-based topologies are already mentioned. Converter Bahravar et al. (2021) discuss the multi-port operation of non-isolated bidirectional DC-DC converter. This converter operation quite similar to boost converter operation but it requires large number of DC sources.

The complete paper is structured in eight sections. Section 1 presents brief introduction covering motivation, challenges and literature review on high gain converters and objectives of paper. Section 2 described the suggested converter configuration and its operational details under CCM and DCM operating modes. Section 3 carried out the design consideration of the converter. The efficiency analysis is discussed in Section 4. State space average modelling of proposed converter is presented in Section 5. Section 6 elaborates the simulation and experimental results in detail. Section 7 analysis the comparative analysis of single switch converters. Finally, Section 8 concludes the theoretical and experimental results.

**Figure 1** Proposed high voltage gain converter

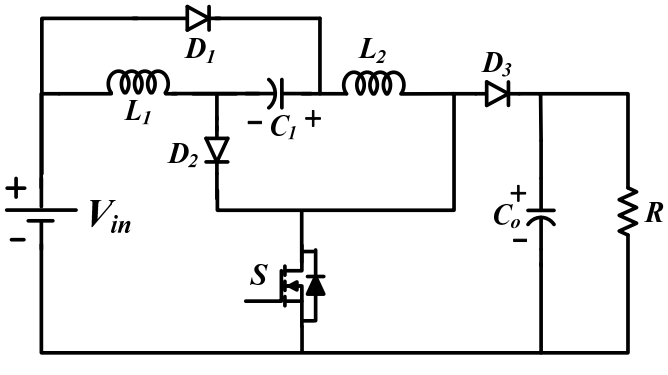


## 2 High gain converter and its operation

Figure 1 represents the structure of suggested high voltage gain converter. It is designed with single switching device ($S$), two capacitors ($C_1$, $C_o$), three diodes ($D_1$, $D_2$, $D_3$) and two inductors ($L_1$, $L_2$). The proposed converter offers only one switching component with less number of elements. This leads reduced cost of converter, low switching losses and ease of control circuitry. Prior to steady state analysis, the few assumptions are made like all the circuit components which include power semiconductor switch and passive elements are considered as ideal components. The output capacitor Co is sufficiently large and therefore, output voltage is constant and ripple-free. The inductors ($L_1$, $L_2$) are identical to L and the current through inductors $L_1$ and $L_2$ are $i_{L1} = i_{L2} = i_L$ and $v_{L1}$, $v_{L2}$ are voltage across inductors respectively. The detailed operation of converter under

continuous conduction and discontinuous conduction modes under steady state operation as follows.

## *2.1 Continuous conduction mode (CCM) operation*

Depending upon the switching states (ON and OFF) of switch (S), two different operating modes under CCM operation are defined.

**Figure 2** Steady state waveforms of voltages and currents under (a) CCM (b) DCM

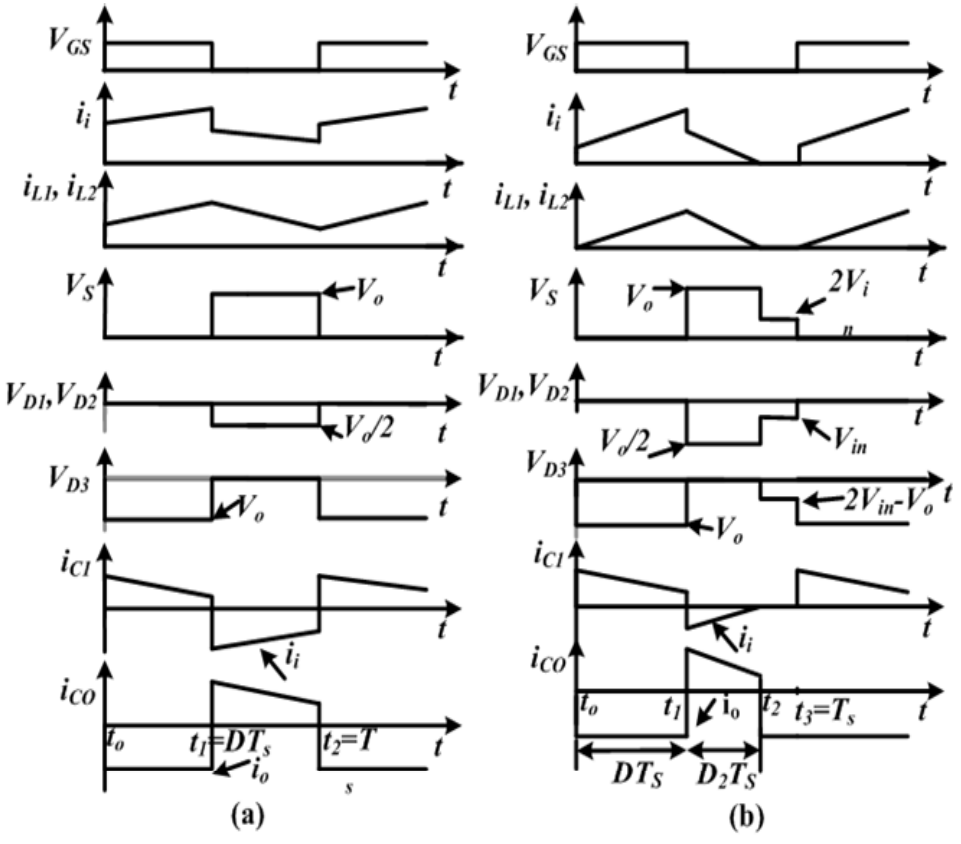


The voltage and current waveforms under CCM operating mode are represented in Figure 2(a) and current paths of these two different modes equivalent circuits are presented in Figure 3(a) and 3(b). The CCM operation is explained in two different modes as given below.

- Mode-1 ($t_0 < t < t_1$): In this interval, the switch ($S$) is turned on and diode $D_3$ is in reverse biased. The diodes ($D_1$, $D_2$) are in forward biased. The. The equivalent circuit depicting the direction of currents paths are given in Figure 3(a). In this mode, the passive components ($C_1$, $L_1$, $L_2$,) are connected in parallel to input voltage ($V_{in}$). Therefore, these components are storing energy. Further, the energy of output capacitor ($C_o$) is delivered to load. Especially in this mode, if capacitor ($C_1$) is

uncharged. It may lead to high inrush current. In order to deal with this issue, the capacitor ($C_1$) is initially pre-charged. Thus, the voltages of energy storage elements $C_1$, $L_1$ and $L_2$ are given below.

$$v_{C1} = v_{L1} = v_{L2} = V_{in} \tag{1}$$

**Figure 3** Equivalent circuits of converter under different switching states, (a) switch ON (b) switch OFF (c) switch OFF in DCM operation (see online version for colours)

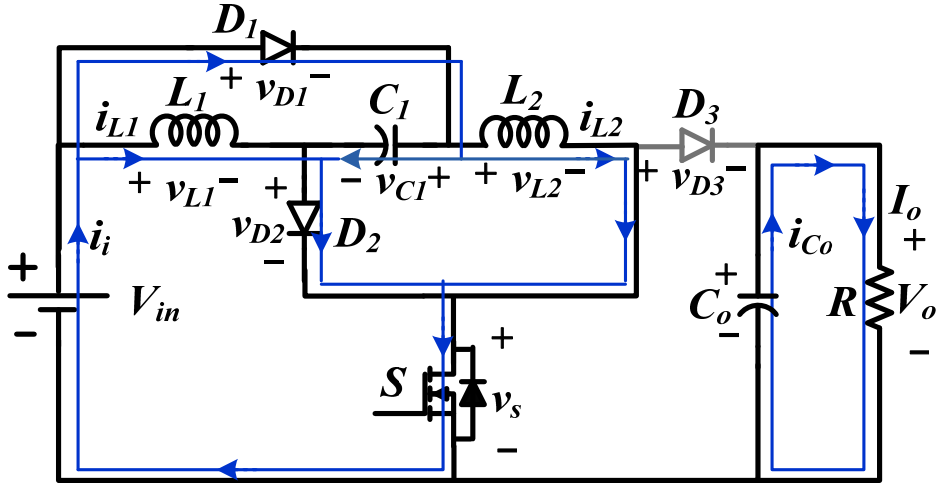


(a)

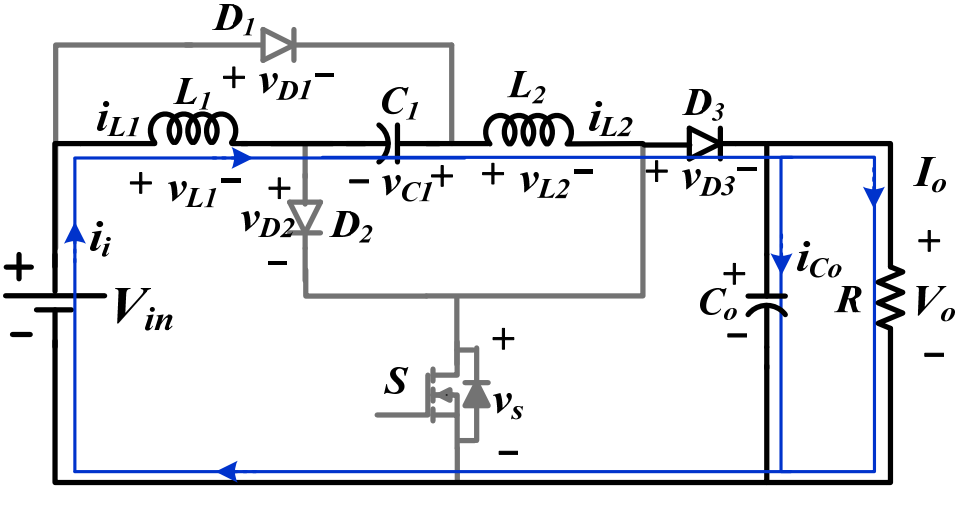


(b)

**Figure 3** Equivalent circuits of converter under different switching states, (a) switch ON (b) switch OFF (c) switch OFF in DCM operation (continued) (see online version for colours)

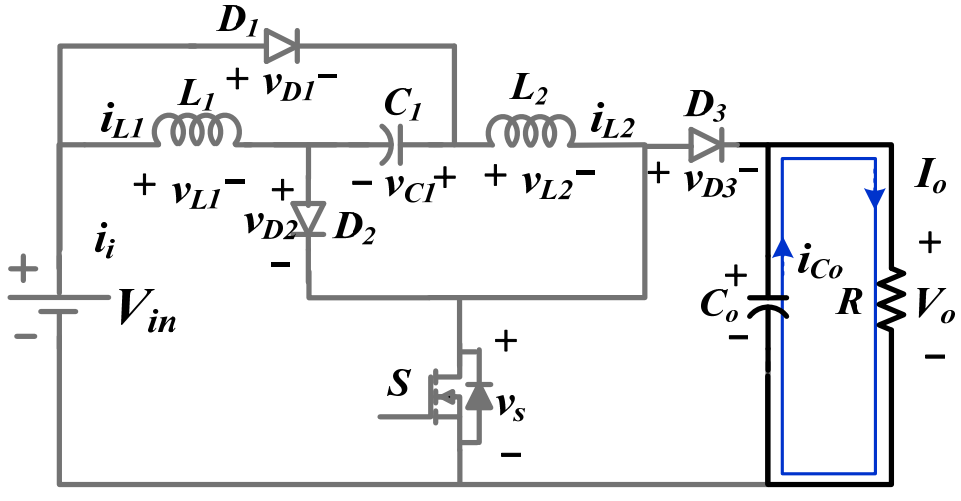


(c)

- Mode-2 ($t_1 < t < t_2$): In this mode switch ($S$) is turned off and diode $D_3$ starts conducting as it is in forward biased. The diodes ($D_1$, $D_2$) are in reverse biased. The. The equivalent circuit representing currents paths are represented in Figure 3(b). The stored energy in the capacitor $C_1$ and inductors ($L_1$, $L_2$) are along with DC input voltage ($V_{in}$) feed power to load and output capacitor $C_o$. Thus, the inductor voltages are expressed as

$$v_{L1} = v_{L2} = \frac{V_{C1} + V_{in} - V_O}{2} \tag{2}$$

$$v_{L1} = v_{L2} = \frac{2V_{in} - V_O}{2} \tag{3}$$

Applying volt-second balance principle across any one of inductor ($L_1$/$L_2$), the equation (4) is obtained.

$$\int_0^{DT_S} V_{in}\,dt + \int_{DT_S}^{T_S} \frac{2V_{in} - V_O}{2}\,dt = 0 \tag{4}$$

From equation (4), the voltage gain of suggested converter under CCM operation is obtained as given in equation (5).

$$M_{CCM} = \frac{V_O}{V_{in}} = \frac{2}{1-D} \tag{5}$$

From Figures 3(a)–3(b), the voltage stress across the switch ($S$), diodes $D_1$, $D_2$ and $D_3$ are obtained as given below.

$$v_S = v_{D3} = V_O \tag{6}$$

$$v_{D1} = v_{D2} = \frac{V_O}{2} \tag{7}$$

## 2.2 Discontinuous conduction mode (DCM) operation

In this subsection, suggested converter operation under DCM mode is discussed. During this operating condition, there are three modes are identified based on the state of switching of switch ($S$) and inductor currents ($i_{L1}$, $i_{L2}$) as depicted in Figure 2(b). The mode-wise detailed discussions are given below:

- Mode-1($t_0 < t < t_1$): In this interval, switch ($S$) and diodes ($D_1$, $D_2$) are in conduction and diode ($D_3$) is non conducting as it is in reverse biased. The current paths of equivalent circuit is represented in Figure 3(a). The voltage and current equations of this mode is given below.

  $$v_{C1} = v_{L1} = v_{L2} = V_{in} \tag{8}$$

  The peak value of each inductor current is obtained at the end of mode-1 as given in equation (9).

  $$I_{L1p} = I_{L2p} = \frac{V_{in}}{L} DT_S \tag{9}$$

- Mode-2 ($t_1 < t < t_2$): In this specific time period, switch ($S$) is turned off. The direction of currents and its equivalent circuit is same as mode-2 of CCM operation. The stored energy in the capacitor $C_1$, inductor $L_1$ and inductor $L_2$ along with DC input voltage are connected to load and output capacitor $C_o$ is charging. At end of mode-2 at $t = t_2$ the energy stored in inductors ($L_1$ and $L_2$) are completely discharged and inductor currents are reached to zero as represented in Figure 2(b). In this mode, peak values of inductor currents ($I_{L1p}$ and $I_{L2p}$) are obtained as given below.

  $$I_{L1p} = I_{L2p} = \frac{V_O - V_{in} - V_{C1}}{2L} D_2 T_S \tag{10}$$

  $$I_{L1p} = I_{L2p} = \frac{V_O - 2V_{in}}{2L} D_2 T_S \tag{11}$$

- Mode-3 ($t_2 < t < t_3$): In this time period switch ($S$) and diodes ($D_1$, $D_2$ and $D_3$) are not conducted and the energy of output capacitor transfer to the load as represented in Figure 3(c). The directions of currents are represented in Figure 3(c). As the energies of two inductors ($L_1$ and $L_2$) are zero and input source ($V_{in}$) are not connected to load. The entire demand of load is met through output capacitor $C_O$. From the equations (9) and (11), the duty cycle ($D_2$) is obtained as given in equation (12).

  $$D_2 = \frac{2V_{in}D}{V_O - 2V_{in}} \tag{12}$$

From Figure 3(b), the output capacitor average current is obtained over one switching period, as given below.

$$i_{C_O} = \frac{\frac{1}{2} D_2 T_S I_{L1p} - I_O T_S}{T_S} \tag{13}$$

Substituting equations (11) and (12) in equation (13), the output capacitor average current is obtained as given in equation (14).

$$i_{C_O} = \frac{D^2 V_{in}^2}{L(V_O - 2V_{in})} - \frac{V_O}{R} \tag{14}$$

As average current through output capacitor under steady state condition is zero, this gives the following conditions.

$$\frac{D^2 V_{in}^2}{L(V_O - 2V_{in})} = \frac{V_O}{R} \tag{15}$$

The voltage gain of converter under DCM operation is obtained by simplification of equation (15). Thus equation (16) is obtained.

$$M_{DCM} = \frac{V_O}{V_{in}} = 1 + \sqrt{1 + \frac{D^2}{\tau_L}} \tag{16}$$

where $\tau_L = \frac{L}{R}$.

It has been observed in DCM that output voltage of converter depends not only on the duty ratio ($D$), but also the circuit parameters like $L$ and $R$.

## 3 Design considerations

In this section, detailed discussion on selection of passive elements like $L_1$, $L_2$, $C_1$ and $C_o$ used in suggested converter are carried out.

### *3.1 Design of inductors ($L_1$, $L_2$)*

The selection of inductors ($L_1$, $L_2$) mainly depends on switching frequency ($f_S$), ripple in inductor current ($\Delta_{iL}$), input voltage ($V_{in}$), and duty ratio ($D$). The design of inductor under CCM operation is obtained by the equation (17).

$$L_{1,Critiical} = L_{2,Critical} = \frac{V_{in} D}{f_S \Delta i_L} \tag{17}$$

### *3.2 Design of output capacitor ($C_o$)*

The selection of output capacitor ($C_o$) depends on output voltage ($V_o$), switching frequency ($f_S$), output power ($P_o$) and output voltage ripple ($\Delta V_C$). The governing equation for the design of output capacitor is given in equation (18).

$$C_{O,Critiical} = \frac{P_o}{V_O \Delta V_C f_S} = \frac{i_O}{\Delta V_C f_S} \tag{18}$$

### 3.3 Design of input capacitor ($C_1$)

The intermediate capacitor ($C_1$) depends on input power ($P_i$), input voltage ($V_{in}$), switching frequency ($f_s$) and voltage ripple ($\Delta V_C$). So, selection of capacitor ($C_1$) is obtained by following equation

$$C_{1,Critiical} = \frac{P_{in}}{V_{in} \Delta V_C f_S} = \frac{i_i}{\Delta V_C f_S} \tag{19}$$

These governing equations for inductors ($L_1$, $L_2$) and capacitors ($C_1$, $C_o$) help to determine actual values for given specifications of high gain converter.

## 4 Efficiency analysis

Figure 4 represents the equivalent circuit of suggested high voltage gain converter. The $r_s$ be the on-state resistance of switch. The resistances of inductors ($L_1$ and $L_2$) are $r_{L1}$ and $r_{L2}$ respectively. The $V_{D1}$, $V_{D2}$ and $V_{D3}$ are forward voltage drops of diodes ($D_1$, $D_2$ and $D_3$) respectively. The internal resistances of diodes ($D_1$, $D_2$, $D_3$) are $r_{D1}$, $r_{D2}$ and $r_{D3}$ respectively. When switch ($S$) is turned on. The average current $I_{Co1}$ through output capacitor and voltage of inductor ($V_{L11}$) during the interval $DT_S$ is written as

$$I_{Co1} = -\frac{V_o}{R} \tag{20}$$

$$V_{L11} = V_{in} - i_{L1}(r_{L1} + r_{D2}) - V_{D2} - i_{in} r_s \tag{21}$$

For the period $(1 - D)T_S$, when switch ($S$) is turned off, the average current ICo2 through output capacitor and the voltage ($V_{L12}$) of inductor for the period of $(1 - D)T_S$ is written as

$$I_{Co2} = i_{L1} - \frac{V_o}{R} \tag{22}$$

$$V_{L12} = \frac{V_{in} - i_{L1}(r_{L1} + r_{L2} + r_{D3}) + V_{C1} - V_{D3} - V_O}{2} \tag{23}$$

As per ampere-second balance theory, the average current of output capacitor is obtained by following equation

$$\int_0^{DT_s} I_{Co1} dt + \int_{DT_s}^{T_s} I_{Co2} dt = 0 \tag{24}$$

Simplification of equation (24) gives the current of inductor $i_{L1}$

$$i_{L1} = \frac{V_o}{R(1-D)} \tag{25}$$

**Figure 4** Equivalent circuit of high voltage gain converter

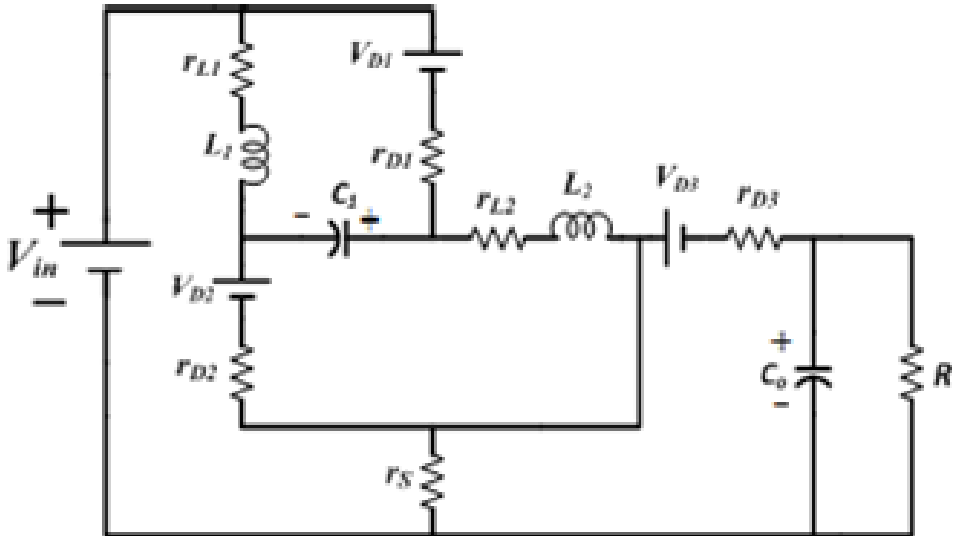


From volt-second balance theory, the inductor average voltage $V_{L1}$ or $V_{L2}$ is obtained by following equation

$$\int_0^{DT_S} V_{L11}dt + \int_{DT_S}^{T_S} V_{L12}dt = 0 \tag{26}$$

From equivalent circuit of converter

$$i_{L1} = i_{L2} = i_{D1} = i_{D2} \tag{27}$$

$$V_{in} = V_{C1} \tag{28}$$

Simplification of equation (26), follows the converter output voltage $V_O$

$$V_O = \frac{2V_{in} - 2V_{D2}D - V_{D3}(1-D)}{(1-D) + \dfrac{1}{R(1-D)}[A+B]} \tag{29}$$

where A = $[2(r_{L1} + r_{D2}) + 4r_s]D$; B = $(r_{L1} + r_{L2} + r_{D3})$ $(1–D)$.

The input power ($P_{in}$) is obtained by

$$P_{in} = V_{in}i_{in} = 2V_{in}i_{L1} \tag{30}$$

The output power ($P_o$) can be obtained by

$$P_O = \frac{V_O^2}{R} - P_{SW} \tag{31}$$

Substituting (25) in (30), the input power is obtained as given below.

$$P_{in} = \frac{2V_{in}V_O}{R(1-D)} \tag{32}$$

Switching losses of converter is obtained by following equation

$$P_{SW} = V_{DS} i_{in} (t_r + t_f) f_{SW} \tag{33}$$

where $P_{SW}$ is switching losses of converter, $V_{DS}$ is voltage between drain and source of MOSFET, $t_r$ is rise time of MOSFET, $i_{in}$ is current of MOSFET, $f_S$ is switching frequency and $t_f$ is fall time of MOSFET.

Using equations (31) to (33), the efficiency of suggested converter can be calculated as given in equation (34).

$$\eta = \frac{P_O}{P_{in}} = \frac{\frac{V_O^2}{R} - P_{SW}}{\left[\frac{2V_{in}V_O}{R(1-D)}\right]} \tag{34}$$

## 5 State space average modelling of proposed converter

The state space average modelling of any system can be obtained by following equations.

$$x^{/} = Ax + Bu \tag{35}$$

$$y = Cx + Du \tag{36}$$

where $x$ is state variable and $x^{l}$ is derivative of state variable of the system. $u$ and $y$ are input and output of the system. $A$, $B$, $C$ and $D$ are system matrixes. In proposed converter the state variable are current passing through inductors ($i_L = i_{L1} = i_{L2}$), voltage across the capacitor $C_1$ and $C_O$ ($V_{C1}$, $V_{CO}$). The CCM operation of proposed converter is operating in two different modes which are shown in Figure 3(a) and 3(b). Following equations are obtained from mode-1 of CCM operation.

$$\frac{di_{L1}}{dt} = \frac{di_{L2}}{dt} = \frac{di_L}{dt} = \frac{V_{in}}{L} \tag{37}$$

$$\frac{dV_{C_O}}{dt} = \frac{-V_{C_O}}{RC_O} \tag{38}$$

$$i_{C_1} = \frac{V_{in}}{Z_{in}} - 2i_L \tag{39}$$

where

$$Z_{in} = \frac{LS}{LC_1S^2 + 2} \tag{40}$$

$$\frac{dV_{C_1}}{dt} = \frac{V_{in}}{Z_{in}C_1} - \frac{2i_L}{C_1} \tag{41}$$

The state equations of CCM operation of mode-1 calculated as follows

$$\begin{bmatrix} i_L^{/} \\ V_{C_1}^{/} \\ V_{C_O}^{/} \end{bmatrix} = [A_1] \begin{bmatrix} i_L \\ V_{C_1} \\ V_{C_O} \end{bmatrix} + [B_1] V_{in} \tag{42}$$

The matrix $A_1$ and $B_1$ are given below

$$[A_1] = \begin{bmatrix} 0 & 0 & 0 \\ \dfrac{-2}{C_1} & 0 & 0 \\ 0 & 0 & \dfrac{-1}{RC_O} \end{bmatrix} \tag{43}$$

$$[B_1] = \begin{bmatrix} \dfrac{1}{L} \\ \dfrac{1}{Z_{in}C_1} \\ 0 \end{bmatrix} \tag{44}$$

Following equations are obtained from CCM operation of Mode-2

$$\frac{di_L}{dt} = \frac{V_{in} + V_{C_1} - V_{C_O}}{2L} \tag{45}$$

$$\frac{dV_{C_1}}{dt} = \frac{-i_L}{C_1} \tag{46}$$

$$\frac{dV_{C_O}}{dt} = \frac{i_L}{C_O} - \frac{V_{C_O}}{RC_O} \tag{47}$$

The state equations of CCM operation of mode-2 calculated as follows

$$\begin{bmatrix} i_L^{/} \\ V_{C_1}^{/} \\ V_{C_O}^{/} \end{bmatrix} = [A_2] \begin{bmatrix} i_L \\ V_{C_1} \\ V_{C_O} \end{bmatrix} + [B_2] V_{in} \tag{48}$$

The matrix $A_2$ and $B_2$ are given below

$$[A_2] = \begin{bmatrix} 0 & \dfrac{1}{2L} & \dfrac{-1}{2L} \\ \dfrac{-1}{C_1} & 0 & 0 \\ \dfrac{1}{C_O} & 0 & \dfrac{-1}{RC_O} \end{bmatrix} \tag{49}$$

$$[B_2] = \begin{bmatrix} \frac{1}{2L} \\ 0 \\ 0 \end{bmatrix} \tag{50}$$

From equations (43), (49), the averaged matrix $A$ is obtained as follows

$$A = A_1 D + A_2 (1 - D) \tag{51}$$

where $D$ is duty cycle of converter

$$[A] = \begin{bmatrix} 0 & \frac{1-D}{2L} & \frac{-(1-D)}{2L} \\ \frac{-(1-D)}{C_1} & 0 & 0 \\ \frac{1-D}{C_O} & 0 & \frac{-1}{RC_O} \end{bmatrix} \tag{52}$$

Equations (44) and (50) gives averaged matrix $B$

$$B = B_1 D + B_2 (1 - D) \tag{53}$$

$$[B] = \begin{bmatrix} \frac{1+D}{2L} \\ \frac{D}{Z_{in} C_1} \\ 0 \end{bmatrix} \tag{54}$$

Output equation of the converter is obtained by equation (55)

$$[V_O] = [0 \quad 0 \quad 1] \begin{bmatrix} i_L \\ V_{C_1} \\ V_{C_O} \end{bmatrix} \tag{55}$$

Average of matrix $C$ is given below

$$C = C_2 D + C_3 (1 - D) \tag{56}$$

where matrix $C_2$ and $C_3$ are equal

$$[C_2] = [C_3] = [0 \quad 0 \quad 1] \tag{57}$$

Transfer function of proposed converter can be obtained by following equation

$$\frac{V_O(S)}{V_{in}(S)} = C[SI - A]^{-1} B \tag{58}$$

$$\frac{V_O(S)}{V_{in}(S)} = \frac{\frac{1}{2LC_O}\left(S(1-D^2)+\frac{(1-D)^2 D}{Z_{in}C_1}\right)}{S^3+\frac{S^2}{RC_O}+\frac{S}{2L}\left(\frac{1-D^2}{C_1}+\frac{(1-D)^2}{C_O}\right)+\frac{1-D^2}{2RLC_1C_O}} \tag{59}$$

## 6 Results and discussion

In this section simulation results for suggested high voltage gain converter is discussed in detailed. Further, to validate the simulation study, equivalent prototype model is developed and its test results are presented.

### *6.1 Simulation results*

The steady state current and voltage waveforms of suggested converter under CCM operation is represented in Figure 5(a). The simulation is carried out for 50 W load on the converter. The switching frequency of gate pulse ($V_{GS}$) is 50 kHz and duty ratio of converter is 50%. The on-state voltage of MOSFET is 0.27 V. 20 V DC be the converter input voltage. The forward voltage drops of diodes are 0.7 V. When switch ($V_S$) is off, the voltage across the switch ($V_S$) is 75.18 V. The peak-to-peak voltage of inductors ($V_{L1}$ and $V_{L2}$) are 38.52 V. The input capacitor ($C_1$) charged to 18.5 V. The average output voltage ($V_o$) of the converter is settled at 75.18 V. The average input current ($i_i$) of converter is 2.41 A. The average current of inductors ($i_{L1}$ and $iL_2$) are 1.191 A. The reverse voltage across the diode ($V_{D3}$) is 75.18 V. The average output current ($i_o$) of the converter is settled at 0.601 A. The reverse voltage across the diodes ($V_{D1}$ and $V_{D2}$) are 37.59 V.

The dynamic state current and voltage waveforms of suggested converter under CCM operation is represented in Figure 5(b). The switching frequency of converter is 50 kHz with 50% duty cycle. From $t$ = 0.25 sec to 0.5 sec, the load on the converter is 45.19 W. The converter draws the input power from the supply is 48.6 W. In the specified time interval the steady state analysis and dynamic state analysis are same. From $t$ = 0.5 sec to 0.75 sec, the converter load is varied from 45.19 W to 36.43 W. The output voltage and current in the specified time period are 75.84 V and 0.4804 A. The converter draws the input power from the supply is 39.4 W. In this time period, input voltage and average input current of converter are 20 V DC and 1.97 A and converter input voltage is 20 V dc. The input capacitor ($C_1$) charged to 18.7 V. The average current of inductors ($i_{L1}$ and $i_{L2}$) are 0.985 A. The voltage stress on the switch is 75.84 V and the reverse voltage across the diode ($D_3$) is 75.84 V and the reverse voltage across the diodes ($D_1$, $D_2$) are 37.92 V. The peak-to-peak voltage of inductor are ($V_{L1}$ and $V_{L2}$) are 38.52 V. From $t$ = 0.75 sec to 1 sec, the converter load is varied from 36.43 W to 26.07 W. The output voltage and current in the specified time period are 76.4 V and 0.33 A. The converter draws the input power from the supply is 27.96 W. In this particular time period the converter input voltage and average input current are 20 V DC and 1.42 A. The input capacitor ($C_1$) charged to 18.9 V. The average current of inductors ($i_{L1}$ and $i_{L2}$) are 0.71 A. The voltage stress on the switch is 76.4 V and the reverse voltage across the diode ($D_3$) is 76.4 V and the reverse voltage across the diodes ($D_1$, $D_2$) are 38.2 V. The peak-to-peak voltage of inductor ($V_{L1}$ and $V_{L2}$) are 38.52 V.

**Figure 5** Proposed converter simulation results (a) steady state analysis (b) dynamic state analysis (see online version for colours)

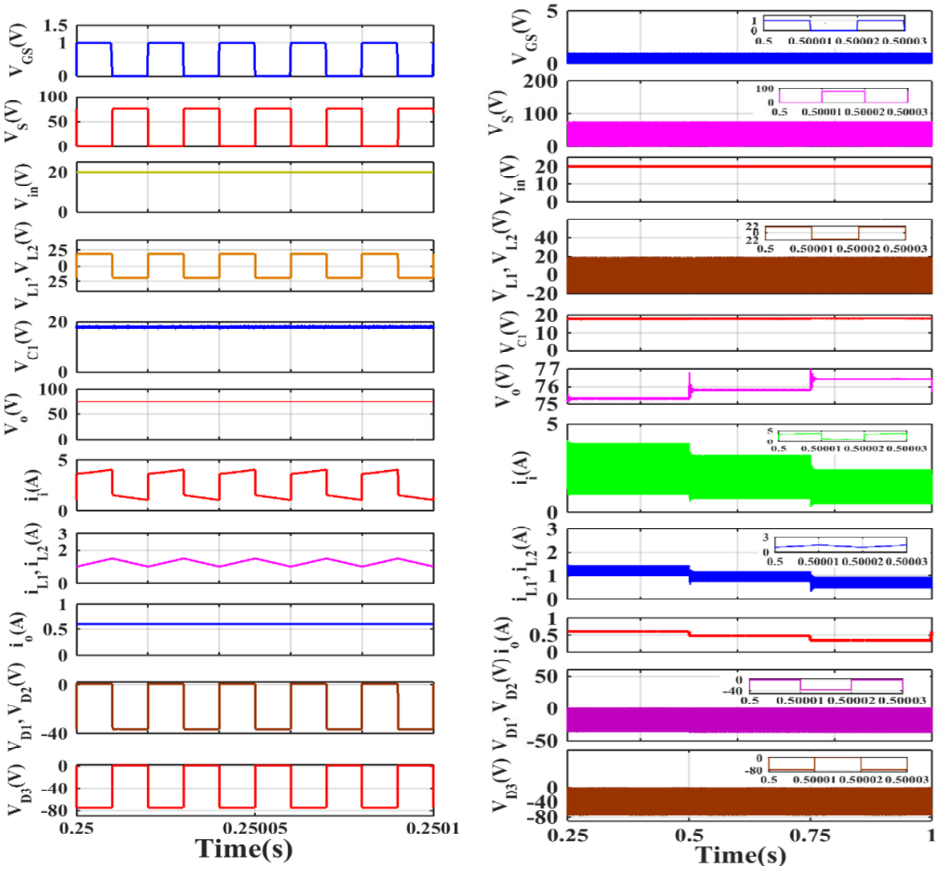


(a) (b)

**Table 1** Specifications of proposed system

| *Parameters* | *Value (unit)* |
|---|---|
| Rated power ($P_o$) | 50 W |
| Input voltage ($V_{in}$) | 20 V |
| Output voltage ($V_o$) | 80 V |
| Duty ratio ($D$) | 0.5 |
| Switching frequency ($f_s$) | 50 kHz |
| Inductors ($L_1$, $L_2$) | 400 µH |
| Capacitor ($C_1$) | 47 µF |
| Capacitor ($C_o$) | 100 µF |
| Power MOSFET ($S$) | IRFP460 |
| Diodes ($D_1$, $D_2$, $D_3$) | STPSC10H065DI |
| Current sensor | LEM (LA25NP:710336) |

**Figure 6** Proposed converter experimental setup (see online version for colours)

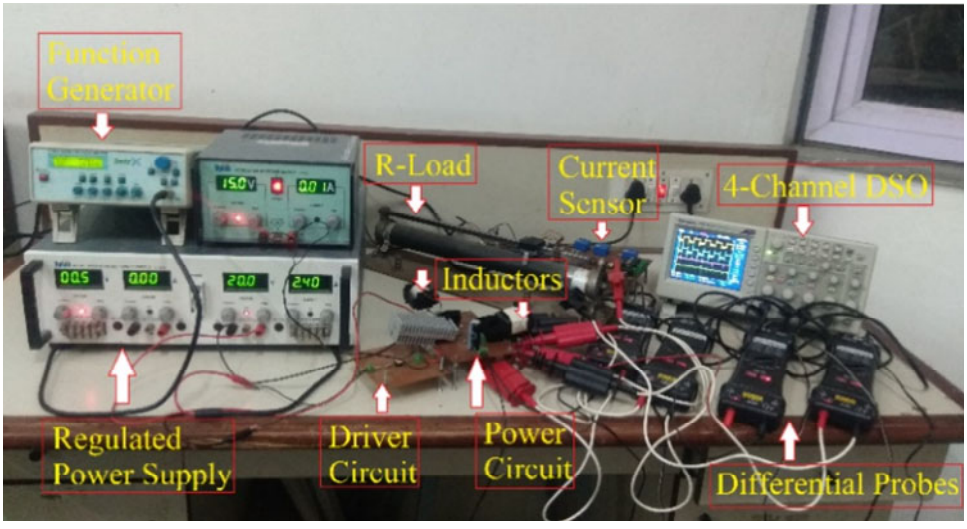


## *6.2 Test results*

A 50 W prototype with specifications tabulated in Table 1 is developed in laboratory environment for validation of theoretical results. The picture of experimental setup is depicted in Figure 6 and it is designed to operate in CCM operation. In order to investigate the performances in steady state conditions, function generator is used to generate the gate pulse for 50% of duty ratio with 50 kHz switching frequency. The IC TLP250 is used as gate driver circuit. The supply voltage is 15 V and peak magnitude of gate pulse at TLP250 input is 2 V. Figure 7(a) represents inductor $L_1$ voltage, inductor $L_2$ voltage, output voltage and capacitor $C_1$ voltage. The converter input voltage is 20 V dc. Inductor $L_1$ and inductor $L_2$ peak to peak voltages are 38 V. Capacitor $C_1$ charged to average voltage of 18.3 V with 5% of ripple. The average output voltage of converter is 74.4 with 1% of ripple. Figure 7(b) represents gate pulse, input voltage and output voltage waveforms. 50 kHz frequency and 15 V peak voltage are assigned to gate pulse and percentage of duty ratio is 50%. Figure 7(c) shows gate pulse, voltage waveforms across diodes ($D_1$, $D_2$). The reverse voltage of diodes $D_1$ and $D_2$ are half of the output voltage, i.e., 37.2 V. Figure 7(d) represents gate pulse, diode $D_3$ and switch (S) voltage waveforms. The switch ($S$) and diode $D_3$ voltages stresses are 74.4 V and –74.4 V. Figure 7(e) shows the gate pulse, inductors $L_1$ and $L_2$ current waveforms. The hall effect current sensor (LEM (LA25NP:710336)) is used for current measurement. The ripple of inductor current is 20% of input current. The average current of inductors ($i_{L1}$ and $i_{L2}$) are 1.22 A (368 mV) and 1.17 A (353 mV). Gate pulse, input and output current waveforms are represented in Figure 7(f). Input current is 2.4 $A$ (720 $mV$) and output current is 0.6 $A$ (180 $mV$). Figure 8 shows various loading conditions of theoretical and experimental output voltages with respect to output power of converter. Experimental and theoretical output voltage of converter at full load are 74.4 V and 75.46 V. Experimental voltage gain at full load is 3.715 and theoretical voltage gain is 3.773. Experimental and theoretical output voltages of converter at low load condition are 76.5 V and 77.4 V.

**Figure 7** Steady state waveform of experimental results (a) inductor voltages ($V_{L1}$, $V_{L2}$), capacitor voltage ($V_{C1}$), output voltage ($V_o$) (b) Gate pulse ($V_{GS}$), input and output voltages ($V_{in}$, $V_o$) (c) gate pulse ($V_{GS}$), diodes voltages ($V_{D1}$, $V_{D2}$) (d) gate pulse ($V_{GS}$), diode voltage ($V_{D3}$), switch voltage ($V_S$) (e) Gate pulse ($V_{GS}$), inductor currents ($i_{L1}$, $i_{L2}$) (f) gate pulse ($V_{GS}$), input and output currents ($i_i$, $i_o$) (see online version for colours)

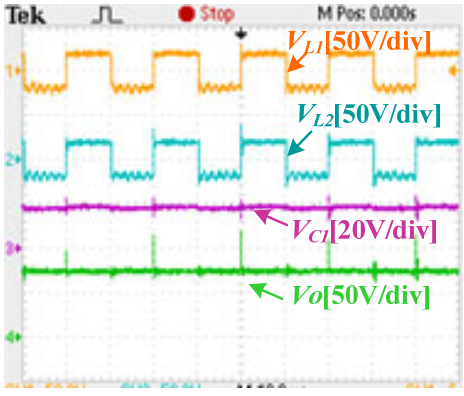


(a)

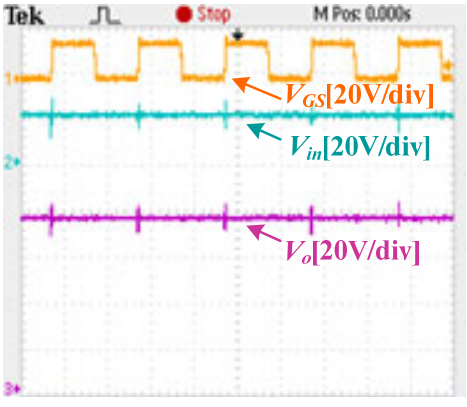


(b)

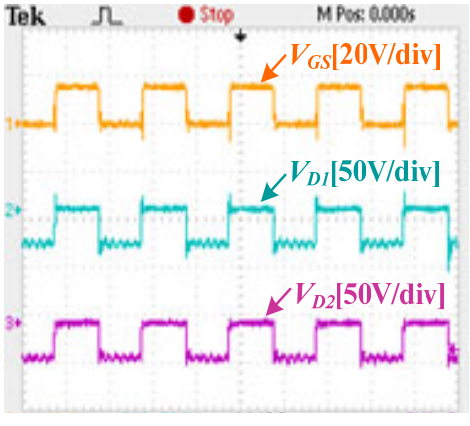


(c)

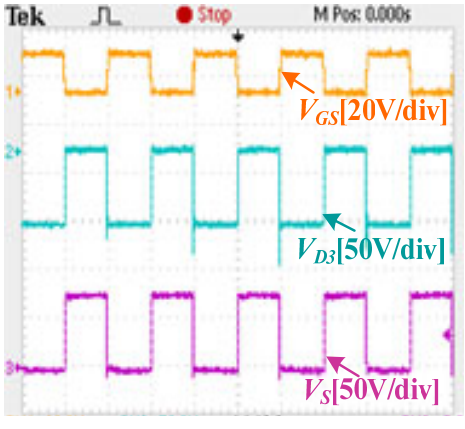


(d)

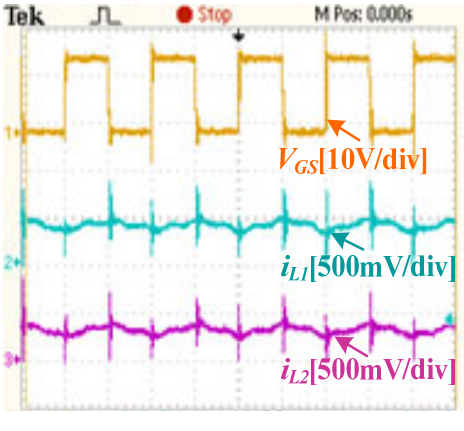


(e)

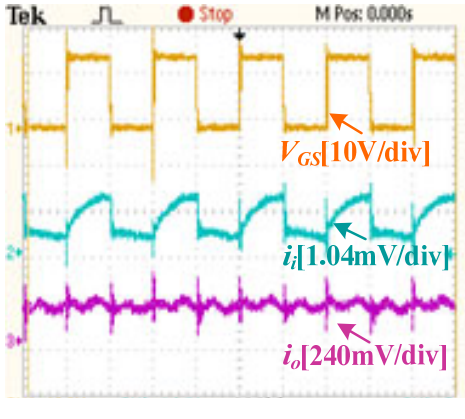


(f)

Figure 9 shows various loading conditions of theoretical and experimental efficiencies with respect to converter output power. The converter experimental and theoretical efficiencies at full load are 92.87% and 93.68%. At low loading condition experimental efficiency is 88.32% whereas theoretical efficiency is 90.10%. The proposed converter maintaining the efficiency above 90% for all loading conditions expect low loading (20W) conditions. The main benefits of suggested converter are: This converter operating on single duty cycle and converter input current is continuous which is more desirable for photovoltaic applications.

**Figure 8** Plot of output voltage versus output power

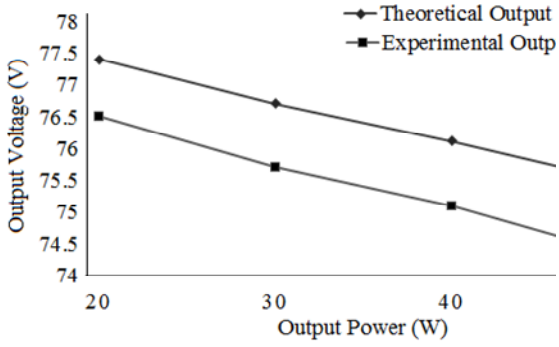


**Figure 9** Plot of efficiency versus output power

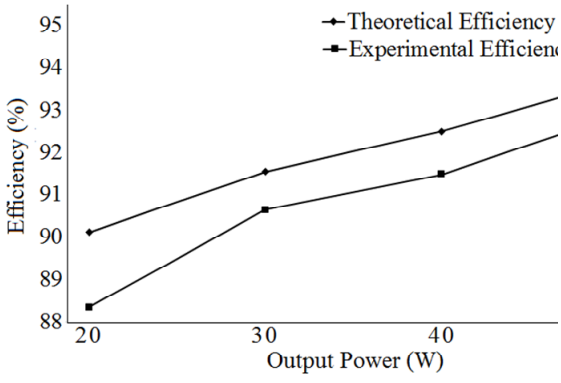


## 7 Performance comparison

The performance comparison of single switch high gain converters and component usage are presented in Table 2. The steady state performances of suggested converter are compared in terms of voltage gain, continuous input current, voltage stress on diodes and switch. From Table 2, the suggested converter gain is high compared to converters (Gules et al., 2014; Banaei et al., 2014; Ismail et al., 2008) and traditional boost converter. The voltage gain verses duty ratio of different single switch converters are plotted in Figure 10. From Figure 10, the proposed converter gives the highest gain of 20 at 0.9

duty ratio whereas converter Gules et al. (2014) gain is 19, converter Banaei et al. (2014) gain is 18, converter Ismail et al. (2008) gain is 11 and boost converter gain is 10 at 0.9 duty ratio. For the suggested converter, the voltage stress on switch ($S$) and diode ($D_3$) are $V_O$ and diodes ($D_1$ and $D_2$) are $\frac{V_O}{2}$. Whereas in converter Banaei et al. (2014), voltage stress on diodes and switch are $\frac{V_O}{2D}$ which is high compared to proposed converter up to 50% of duty ratio. High gain converters are cannot operate at extreme duty cycle due to recovery of diodes. Diode voltage stress of proposed converter is less compared to converter Gules et al. (2014). The number of switches in proposed converter, converters Gules et al. (2014), Banaei et al. (2014), Ismail et al. (2008) and boost converter are same. Number of inductors, total device count in proposed converter, converters Gules et al. (2014), Banaei et al. (2014); Ismail et al. (2008) are same. Number of diodes in proposed converter and converter Ismail et al. (2008) are same. Number of capacitors in proposed converter and converter Ismail et al. (2008) are same whereas in converter Gules et al. (2014) and Banaei et al. (2014) are three. The efficiency of converters proposed in Gules et al. (2014), Ismail et al. (2008) are 91.9% and 92.1% respectively. At nominal loading condition, the proposed converter efficiency is 92.87% which is higher than the converters proposed in Gules et al. (2014) and Ismail et al. (2008). Except converter Banaei et al. (2014) and Ismail et al. (2008), remaining all converters are following continuous input current which is desirable for photovoltaic applications.

**Table 2** Performance comparison of proposed high voltage gain converter

| *Parameters* | *Proposed* | *Gules et al. (2014)* | *Banaei et al. (2014)* | *Ismail et al. (2008)* | *Boost* |
|---|---|---|---|---|---|
| Voltage gain | $\frac{2}{1-D}$ | $\frac{1+D}{1-D}$ | $\frac{2D}{1-D}$ | $\frac{2-D}{1-D}$ | $\frac{1}{1-D}$ |
| Voltage stress on switches | $V_O$ | $\frac{V_o}{1+D}$ | $\frac{V_o}{2D}$ | $\frac{V_o}{2-D}$ | $V_O$ |
| Voltage stress on diodes | $\frac{V_o}{2}$ | $\frac{V_o}{1+D}$ | $\frac{V_o}{2D}$ | $\frac{V_o}{2-D}$ | $V_O$ |
| Number of switches | 1 | 1 | 1 | 1 | 1 |
| Number of diodes | 3 | 2 | 2 | 3 | 1 |
| Number of inductors | 2 | 2 | 2 | 1 | 1 |
| Number of capacitors | 2 | 3 | 3 | 3 | 1 |
| Total device count | 8 | 8 | 8 | 8 | 4 |
| Continuous input current | Yes | Yes | No | No | Yes |

**Figure 10** Comparison of high voltage gain converters

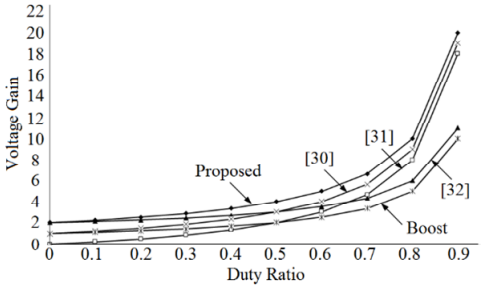


## 8 Conclusions

In this paper a single switch non-isolated high voltage gain and high efficiency DC-DC converter is offered. The suggested converter can be used for photovoltaic systems in DC microgrid. Most of the photovoltaic systems MPPT control working on single duty ratio. So, this converter offers single duty ratio with continuous input current which is necessary requirement for photovoltaic systems. The suggested converter voltage gain, switching device voltage stress and usage of components are compared with existing single switch high voltage gain converters. The suggested converter voltage gain is high compared to converter Gules et al. (2014), Banaei et al. (2014) and Ismail et al. (2008). The theoretical efficiency analysis of suggested converter is evaluated. A 50 W prototype experimental setup is developed for confirmation of theoretical results. The voltage gain and full load efficiency of the converter are 3.72 and 92.87% which are very close to theoretical values.

## References

Ajami, A., Ardi, H. and Farakhor, A. (2015) 'A novel high step-up DC/DC converter based on integrating coupled inductor and switched capacitor techniques for renewable energy applications', *IEEE Trans. Power Electron.*, Vol. 30, No. 8, pp.4255–4263.

Ardi, H. and Ajami, A. (2018) 'Study on a high voltage gain SEPIC-based DC-DC converter with continuous input current for sustainable energy applications', *IEEE Trans. Power Electron.*, Vol. 33, No. 12, pp.10403–10409.

Ardi, H., Ajami, A. and Sabahi, M. (2018) 'A novel high step-up DC–DC converter with continuous input current integrating coupled inductor for renewable energy applications', *IEEE Trans. Ind. Electron.*, Vol. 65, No. 2, pp.1306–1315.

Axelrod, B., Berkovich, Y. and Ioinovici, A. (2008) 'Switched-capacitor/switched-inductor structures for getting transformerless hybrid DC–DC PWM converters', *IEEE Trans. Circuits Syst. I, Reg. Papers*, Vol. 55, No. 2, pp.687–696.

Baddipadiga, B.P. and Ferdowsi, M. (2017) 'A high-voltage-gain DC-DC converter based on modified dickson charge pump voltage multiplier', *IEEE Trans. Power Electron.*, Vol. 32, No. 10, pp.7707–7715.

Bahravar, S., Abbaszadeh, K. and Olamaei, J, (2021) 'A multi-port non-isolated bidirectional DC-DC converter', *Int. J. Power Electronics*, Vol. 15, No. 1, pp.86–115.

Banaei, M.R. and Sani, S.G. (2018) 'Analysis and implementation of a new SEPIC-based single switch buck-boost dc-dc converter with continuous input current', *IEEE Trans. Power Electron*., Vol. 33, No. 12, pp.10317–10325.

Banaei, M.R., Ardi, H. and Farakhor, A. (2014) 'Analysis and implementation of a new single-switch buck–boost DC/DC converter', *IET Power Electron*., Vol. 7, No. 7, pp.1906–1914.

Berkovich, Y. and Axelrod, B. (2011) 'Switched-coupled inductor cell for DC–DC converters with very large conversion ratio', *IET Power Electron*., Vol. 4, No. 3, pp.309–315.

Bryant, B. and Kazimierczuk, M.K. (2007) 'Voltage-loop power stage transfer functions with MOSFET delay for boost PWM converter operating in CCM', *IEEE Trans. Ind. Electron*., Vol. 54, No. 1, pp.347–353.

Carrasco, J.M. et al. (2006) 'Power-electronic systems for the grid integration of renewable energy sources: a survey', *IEEE Trans. Ind. Electron.*, Vol. 53, No. 4, pp.1002–1016.

Chen, S.M., Lao, M-L., Hsieh, Y-H., Liang, T-J. and Chen, K-H. (2015) 'A novel switched coupled-inductor DC–DC step-up converter and its derivatives', *IEEE Trans. Ind. Appl.*, Vol. 51, No. 1, pp.309–314.

Choi, J., Cha, H. and Han, B-M. (2010) 'A three-phase interleaved DC–DC converter with active clamp for fuel cells', *IEEE Trans. on Power Electron*., Vol.25, No. 8, pp.2115–2123.

Eghtedarpour, N. and Farjah, E. (2014) 'Distributed charge/discharge control of energy storages in a renewable-energy-based DC micro-grid', *IET Renewable Power Generation*., Vol. 8, No. 1, pp.45–57.

Forouzesh, M., Yari, K., Baghramian, A. and Hasanpour, S. (2017) 'Single-switch high step-up converter based on coupled inductor and switched capacitor techniques with quasi-resonant operation', *IET Power Electron*., Vol. 10, No. 2, pp.240–250.

Gules, R., Dos Santos, W.M., Dos Reis, F.A., Romaneli, E.F.R. and Badin, A.A. (2014) 'A modified SEPIC converter with high static gain for renewable applications', *IEEE Trans. Power Electron.*, Vol. 29, No. 11, pp.5860–5871.

Hart, D.W. (2011) *Power Electronics (series 1)*, 1st ed., February, Vol. 1, No. 7, pp.196–259, McGraw-Hill, New York, NY, USA.

Ismail, E.H., Al-Saffar, M.A., Sabzali, A.J. and Fardoun, A.A. (2008) 'A family of single-switch PWM converters with high step-up conversion ratio', *IEEE Trans. Circuits Syst. I*, Reg. Papers, Vol. 55, No. 4, pp.1159–1171.

Lakshmi, M. and Hemamalini, S. (2018) 'Nonisolated high gain DC–DC converter for DC microgrids', *IEEE Trans. Ind. Electron.*, Vol. 65, No. 2, pp.1205–1212.

Lee, S.W. and Do, H-L. (2018) 'Isolated SEPIC DC–DC converter with ripple free input current and lossless snubber', *IEEE Trans. Ind. Electron*., Vol. 65, No. 2, pp.1254–1262.

Li, W. and He, X. (2011) 'Review of nonisolated high-step-up DC/DC converters in photovoltaic grid-connected applications', *IEEE Trans. Ind. Electron.*, Vol. 58, No. 4, pp.1239–1250.

Luo, F.L. and Ye, H. (2004) 'Positive output cascade boost converters', *IEE Proc.-Elect. Power Appl.*, Vol. 151, No. 5, pp.590–606.

Mantovanelli, P. and Barbi, I. (1996) 'A new current-fed, isolated PWM DC-DC converter', *IEEE Trans. on Power Electron*., Vol. 11, No. 3, pp.431–438.

Mohammadi, M., Taheri, M., MiliMonfared, J., Abbasi, B. and Behbahani, M.R.M. (2014) 'High step-up DC-DC converter with ripple free input current and soft switching', *IET Power Electron.*, Vol. 7, No. 12, pp.3023–3032.

Moradpour, R., Ardi, H. and Tavakoli, A. (2018) 'Design and implementation of a new SEPIC-based high step-up DC/DC converter for renewable energy applications', *IEEE Trans. Ind. Electron*., Vol. 65, No. 2, pp.1290–1297.

Nguyen, M.K., Duong, T-D., Lim, Y-C. and Kim, Y-J. (2018) 'Isolated boost DC–DC converter with three switches', *IEEE Trans. Power Electron.*, Vol. 33, No. 2, pp.1389–1398.

Park, K.B., Moon, G-W. and Youn, M-J. (2010) 'Nonisolated high step up boost converter integrated with SEPIC converter', *IEEE Trans. Power Electron*., Vol. 25, No. 9, pp.2266–2275.

Prudente, M., Pfitscher, L.L., Emmendoerfer, G., Romaneli, E.F. and Gules, R. (2008) 'Voltage multiplier cells applied to non-isolated DC–DC converters', *IEEE Trans. Power Electron.*, Vol. 23, No. 2, pp.871–887.

Salvador, M.A., Lazzarin, T.B. and Coelho, R.F. (2018) 'High step-up DC–DC converter with active switched-Inductor and passive switched-capacitor networks', *IEEE Trans. Ind. Electron*., Jul. 2018, Vol. 65, No. 7, pp.5644–5654.

Tofoli, F.L., de Souza Oliveira, D., Torrico-Bascop´e, R.P. and Alcazar, Y.\J.A. (2012) 'Novel nonisolated high-voltage gain DC–DC converters based on 3SSC and VMC', *IEEE Trans. Power Electron.*, Vol. 27, No. 9, pp.3897–3907.

Tofoli, F.L., Pereira, D.D.C., Josias de Paula, W. and Oliveira J´unior, D.D.S. (2015) 'Survey on non-isolated high-voltage step-up dc–dc topologies based on the boost converter', *IET Power Electron*., Vol. 8, No. 10, pp.2044–2057.

Vesali, M., Delshad, M. and Naeini, A.K. (2021) 'A new high step-up soft switching converter for photovoltaic system', *Int. J. Power Electronics*, Vol. 15, No. 1, pp.131–140.

Wai, R.J., Lin, C-Y., Duan, R-Y. and Chang, Y-R. (2007) 'High-efficiency DC-DC converter with high voltage gain and reduced switch stress', *IEEE Trans. Ind. Electron*., Vol. 54, No. 1, pp.354–364.

Wu, X., Zhang, J., Ye, X. and Qian, Z. (2008) 'Analysis and derivations for a family ZVS converter based on a new active clamp ZVS cell', *IEEE Trans. Ind. Electron*., Vol. 55, No. 2, pp.773–781.

Zhu, M. and Luo, F. (2008) 'Series SEPIC implementing voltage-lift technique for DC–DC power conversion', *IET Power Electron.*, Vol. 1, No. 1, pp.109–121.